

A Four-Dimensional Incremental Analysis Update for the Ensemble Kalman Filter

LILI LEI

Key Laboratory of Mesoscale Severe Weather, Ministry of Education, and School of Atmospheric Sciences, Nanjing University, Nanjing, China, and Cooperative Institute for Research in Environmental Sciences, University of Colorado Boulder, Boulder, Colorado

JEFFREY S. WHITAKER

NOAA/Earth System Research Laboratory/Physical Sciences Division, Boulder, Colorado

(Manuscript received 10 July 2015, in final form 7 April 2016)

ABSTRACT

The analysis produced by the ensemble Kalman filter (EnKF) may be dynamically inconsistent and contain unbalanced gravity waves that are absent in the real atmosphere. These imbalances can be exacerbated by covariance localization and inflation. One strategy to combat the imbalance in the analyses is the incremental analysis update (IAU), which uses the dynamic model to distribute the analyses increments over a time window. The IAU has been widely used in atmospheric and oceanic applications. However, the analysis increment that is gradually introduced during a model integration is often computed once and assumed to be constant for an assimilation window, which can be seen as a three-dimensional IAU (3DIAU). Thus, the propagation of the analysis increment in the assimilation window is neglected, yet this propagation may be important, especially for moving weather systems.

To take into account the propagation of the analysis increment during an assimilation window, a four-dimensional IAU (4DIAU) used with the EnKF is presented. It constructs time-varying analysis increments by applying all observations in an assimilation window to state variables at different times during the assimilation window. It then gradually applies these time-varying analysis increments through the assimilation window. Results from a dry two-layer primitive equation model and the NCEP GFS show that EnKF with 4DIAU (EnKF-4DIAU) and 3DIAU (EnKF-3DIAU) reduce imbalances in the analysis compared to EnKF without initialization (EnKF-RAW). EnKF-4DIAU retains the time-varying information in the analysis increments better than EnKF-3DIAU, and produces better analysis and forecast than either EnKF-RAW or EnKF-3DIAU.

1. Introduction

Data assimilation seeks to find the best estimate of the state of a dynamical system given a forecast model and observations of the system (Kalnay 2002). The ensemble Kalman filter (EnKF; Evensen 1994; Burgers et al. 1998), a Monte Carlo approximation to the traditional Kalman filter (KF; Kalman 1960), uses an ensemble of forecasts to estimate the covariances between state variables and observations, which determines the increment to the state estimate given the observations.

Because of its simplicity of implementation and maintenance and its ability to estimate the flow-dependent background-error covariances, the EnKF has been increasingly used in numerical weather prediction (e.g., Whitaker et al. 2008; Houtekamer and Mitchell 2005; Buehner et al. 2010a,b).

However, the analysis produced by the EnKF may be dynamically inconsistent and contain gravity waves that are absent in the real atmosphere and may contaminate the subsequent forecast. These imbalances can be generated by covariance localization and inflation. Covariance localization was introduced by Houtekamer and Mitchell (2001) and Hamill et al. (2001) to mitigate the impact of spurious correlations due to limited ensemble sizes (Mitchell et al. 2002; Houtekamer and Mitchell 2005) but can degrade balances between

Corresponding author address: Lili Lei, School of Atmospheric Sciences, Nanjing University, 163 Xianlin Ave., Nanjing 210023, China.
E-mail: lililei@nju.edu.cn

variables in the background ensemble (Kepert 2009; Greybush et al. 2011). Covariance inflation inflates the prior or posterior ensemble to avoid the filter divergence (Anderson and Anderson 1999) but can degrade balances if different inflation factors are applied to different state variables, which can occur in the methods described by Zhang et al. (2004), Anderson (2009), and Whitaker and Hamill (2012).

Several strategies to combat the imbalance in the EnKF analyses have been developed. Normal mode initialization (Machenhauer 1977; Baer and Tribbia 1977) and digital filtering (DFI; Lynch and Huang 1992; Huang and Lynch 1993) employ a balancing procedure after the data assimilation step. Besides the post-processing methods, several approaches have been proposed to render the assimilation procedure more dynamically consistent. Bloom et al. (1996) introduced the method of incremental analysis update (IAU) that distributes the analyses increments over a fixed time window. Bergemann and Reich (2010) proposed a “mollified” EnKF, which creates balanced analyses by using a continuous formulation of the Kalman filter. Lei et al. (2012a,b) developed a hybrid nudging EnKF that applies the EnKF gradually in time via nudging-type terms to achieve better temporal smoothness and reduce the data insertion shocks. Gottwald (2014) introduced a weak constraint on the imbalance and controlled the unbalanced fast dynamics in the EnKF. Kepert (2009) modified the covariance localization in EnKF to better preserve geostrophic balance in the ensemble.

Since the IAU was originally proposed by Bloom et al. (1996), it has been frequently used in atmospheric data assimilation (e.g., Zhu et al. 2003; Rienecker et al. 2007). Later, diverse varieties of IAU have been developed in oceanic data assimilation (e.g., Carton et al. 2000; Ourmières et al. 2006). It has been demonstrated that the IAU scheme that incorporates the analysis increment in a gradual manner can keep the mass and momentum fields in dynamical balance and reduce the spurious oscillations produced in the data assimilation. One difference among the IAU techniques is the time window of the increment application. For instance, Carton et al. (2000) computed the increment at the center of the assimilation window and applied this increment in the assimilation window. Ourmières et al. (2006) and Huang et al. (2002) computed the increment at the end of assimilation window, but the former applied the increment inside the current assimilation window while the latter applied the increment inside the next assimilation window. Another difference among the IAU techniques is the weighting function (Polavarapu et al. 2004). Yan et al. (2014) compared different IAU implementations, including variations in

the time window and the weighting function, using an EnKF applied to an ocean circulation model.

All of the IAU schemes just discussed use a single increment that is assumed constant over an assimilation window during model integration. We call this three-dimensional IAU (3DIAU). The propagation of the increment in the assimilation window is neglected, yet this propagation may be important, especially for fast-moving weather systems (such as recurving tropical cyclones).

To remedy this, a four-dimensional IAU (4DIAU) was recently proposed by Lorenc et al. (2015). In a 6-h assimilation window, hourly analysis increments without time interpolation were used to filter out the high-frequency oscillations introduced by the four-dimensional ensemble variational method (4DEnVar) at the Met Office. The 4DIAU used with 4DEnVar performed well compared to the 4DVAR that applies a digital time filter to the increment trajectory by including a penalty term J_c . The 4DVAR J_c term is not applicable for 4DEnVar, since the increments of 4DEnVar are not explicitly propagated with a tangent linear model. Buehner et al. (2015) discussed the replacement of the existing full-field digital filter with the 4DIAU for the 4DEnVar at the Environment Canada. They found that the 4DIAU significantly reduced the model spinup and produced an improved representation of the semidiurnal tide.

Comparing to 3DIAU, 4DIAU constructs time-varying analysis increments by applying all observations in an assimilation window to state variables at different times during the assimilation window. These time-varying analysis increments translate into time-varying forcing terms in the forecast model integration during the application of IAU. The 4DIAU is investigated with the EnKF in this study. The 4DIAU helps to reduce the imbalance caused by the EnKF and retain the propagation of analysis increments compared to 3DIAU. A dry two-layer primitive equation model (Zou et al. 1993) and the NCEP Global Forecast System (GFS) are used here. Using the two-layer model, the differences between 3DIAU and 4DIAU with EnKF are examined, and the sensitivities of the 3DIAU and 4DIAU with EnKF on observation network, model error, ensemble size, and frequency of analysis increment are also explored. Then the 3DIAU and 4DIAU are further compared using the NCEP GFS with real observations, and they are also compared to a DFI that is the same as that in the operational Global Data Assimilation System (GDAS).

The structure of this paper is as follows. Section 2 describes the 4DIAU method. Section 3 describes the two-layer model and experimental design. The results from the two-layer model are discussed in section 4. The design of experiments with the NCEP GFS is explained

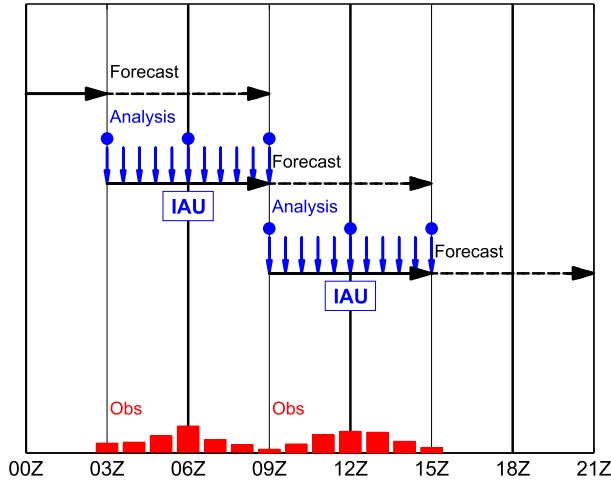


FIG. 1. Schematic illustration of the 4DIAU algorithm.

in section 5, and results from the NCEP GFS experiments are presented in section 6. The conclusions are summarized in section 7.

2. Methodology

Figure 1 displays the schematic of the 4DIAU. For the current assimilation window (0300–0900 UTC), a forecast (or an ensemble of forecasts) is made from the analysis (analyses) at the end of previous assimilation window (0300 UTC). Observations (red bars) are inhomogeneously distributed during the assimilation window. As an example, three analyses (blue dots) are constructed by applying all observations in the assimilation window to the state variables at the beginning, middle, and end of the assimilation window, respectively. More frequent analyses during the assimilation window could be constructed to better represent the time variation of analysis increments (the sensitivity of the 4DIAU to the analysis increment frequency will be discussed in sections 4 and 6). Any four-dimensional data assimilation approach can be used to construct the analyses, including ensemble-based methods (e.g., Anderson 2001; Whitaker and Hamill 2002; Hunt et al. 2007), variational methods (e.g., Lorenc 1986; Courtier et al. 1998; Thepaut et al. 1993), and ensemble-variational methods (e.g., Buehner et al. 2010a,b; Wang et al. 2013; Wang and Lei 2014). Let \mathbf{x}_t^f and \mathbf{x}_t^a denote the forecast and analysis at time t , and the analysis increment at time t is $\Delta\mathbf{x}_t = \mathbf{x}_t^a - \mathbf{x}_t^f$. Linearly interpolate the three analysis increments ($\Delta\mathbf{x}_{0300}$, $\Delta\mathbf{x}_{0600}$, and $\Delta\mathbf{x}_{0900}$) to every model time step from 0300 to 0900 UTC to obtain the time-varying analysis increments $\Delta\mathbf{x}_t$ for the current assimilation window. The time-varying IAU forcing terms $\Delta\mathbf{x}_t/\Delta t$ (blue arrows) where Δt denotes the length of the assimilation window are then added to the

tendency terms during the model integration from 0300 to 0900 UTC. Free model integration continues through the next assimilation window. These procedures repeat for each assimilation cycle.

For comparison, 3DIAU (Bloom et al. 1996) only uses the analysis increment in the middle of the window (0600 UTC) and translates this increment into constant forcing terms along the model integration from 0300 to 0900 UTC, while 4DIAU uses multiple analysis increments in the assimilation window and considers the propagation of the analysis increment during the assimilation window.

Bloom et al. (1996) and Polavarapu et al. (2004) used a linear model to analyze the filtering properties of 3DIAU. Since IAU acts only to filter the increments and not the background state, the filter response function is usually computed as the ratio of the increment integrated over the assimilation window for IAU and intermittent assimilation [the second terms of Eqs. (11) and (12) of Polavarapu et al. (2004)]. Here we consider the filtering properties of 4DIAU relative to 3DIAU by computing the ratio of the increment integrated over the assimilation window for 3DIAU and 4DIAU.

In Polavarapu et al. (2004) a general linear model is considered, to simplify the analysis we consider a simple oscillation equation with a single frequency ω , and assume the weights used for the IAU forcing are constant through the assimilation window. The model state at time t is

$$f(\mathbf{x}, t) = A \cos \left[k\mathbf{x} - \omega \left(t - \frac{\Delta t_c}{2} \right) \right], \quad (1)$$

where A , k , ω , and Δt_c are constants. The true state is shifted relative to the model state by Δt_c , and is given by

$$f^t(\mathbf{x}, t) = A \cos \left[k\mathbf{x} - \omega \left(t + \frac{\Delta t_c}{2} \right) \right]. \quad (2)$$

The forecast error at time t is

$$\Delta f(\mathbf{x}, t) = f^t(\mathbf{x}, t) - f(\mathbf{x}, t) = 2A \sin(k\mathbf{x} - \omega t) \sin \left(\omega \frac{\Delta t_c}{2} \right). \quad (3)$$

Following Polavarapu et al. (2004), the integral of the 3DIAU forcing $\Delta f(\mathbf{x}, t_c)$ over the assimilation window ($t_c - \tau/2, t_c + \tau/2$), where τ is the forecast length, is

$$\begin{aligned} \Delta \tilde{f}(\mathbf{x})_{3\text{DIAU}} &= \int_{t=t_c-\tau/2}^{t=t_c+\tau/2} \frac{\Delta f(\mathbf{x}, t_c)}{\tau} dt \\ &= 2A \sin(k\mathbf{x} - \omega t_c) \sin \left(\omega \frac{\Delta t_c}{2} \right), \end{aligned} \quad (4)$$

where τ in the denominator is a normalization factor to apply the analysis increment at every time step within the assimilation window.

In 4DIAU, if there are N increments within the assimilation window, the integral of the forcing $\Delta f(\mathbf{x}, t)$ can be approximated with the trapezoidal rule as

$$\Delta \tilde{f}(\mathbf{x})_{4\text{DIAU}} = \frac{1}{N-1} \sum_{j=1}^{N-1} \frac{\Delta f \left[\mathbf{x}, t_c - \frac{\tau}{2} + \frac{(j-1)\tau}{N-1} \right] + \Delta f \left(\mathbf{x}, t_c - \frac{\tau}{2} + \frac{j\tau}{N-1} \right)}{2}. \quad (5)$$

Substituting (3) into (5) and dividing by (4) gives

$$\frac{\Delta \tilde{f}(\mathbf{x})_{4\text{DIAU}}}{\Delta \tilde{f}(\mathbf{x})_{3\text{DIAU}}} = R = \frac{1}{N-1} \left\{ 1 + \cos\theta + 2 \sum_{i=1}^{[(N-1)/2]-1} \cos \left[\frac{i}{(N-1)/2} \theta \right] \right\}, \quad (6)$$

where $\theta = \omega(\tau/2)$.

The ratio of 4DIAU and 3DIAU forcing integrated over the assimilation window is a function of N and θ . To

isolate the impact of the number of time levels used to compute the IAU forcing (N), we average over all possible θ to obtain the following:

$$\begin{aligned} \frac{\int_0^{\theta_{\text{Nyquist}}} \Delta \tilde{f}(\mathbf{x})_{4\text{DIAU}}}{\int_0^{\theta_{\text{Nyquist}}} \Delta \tilde{f}(\mathbf{x})_{3\text{DIAU}}} &= \tilde{R} = \frac{\int_0^{\theta_{\text{Nyquist}}} \frac{1}{N-1} \left\{ 1 + \cos\theta + 2 \sum_{i=1}^{[(N-1)/2]-1} \cos \left[\frac{i}{(N-1)/2} \theta \right] \right\} d\theta}{\int_0^{\theta_{\text{Nyquist}}} d\theta} \\ &= \frac{\frac{\theta_{\text{Nyquist}}}{N-1} + \frac{\sin(\theta_{\text{Nyquist}})}{N-1} + \sum_{i=1}^{[(N-1)/2]-1} \frac{1}{i} \sin \left[\frac{i}{(N-1)/2} \theta_{\text{Nyquist}} \right]}{\theta_{\text{Nyquist}}}, \end{aligned} \quad (7)$$

where θ_{Nyquist} is the Nyquist frequency (determined by the forecast model time step).

Figure 2 shows \tilde{R} as a function of N for $\theta_{\text{Nyquist}} = 2000\pi$. 4DIAU acts as a weaker time filter than 3DIAU, and the degree of filtering decreases as N increases. The time filtering of analysis increments in 4DIAU arises from the smoothing associated with the interpolation of the forcing from the discrete number N of times at which it is available to the model time step. As the interval at which the analysis increment is computed approaches the model time step, the filtering effects of 4DIAU vanish. Therefore, the ultimate choice of N is likely to reflect a balance between choosing N small enough to filter out unwanted high-frequency oscillations excited by the analysis increments, and choosing N large enough to avoid adversely affecting the propagation of the true “signal” associated with the propagation of predictable, synoptic-scale analysis increments through the assimilation window. The time filtering of 4DIAU can be possibly retained with a large N , if the weights for the analysis increments of 4DIAU are nonuniform through the assimilation window. If there is significant propagation of analysis increments within the assimilation window,

3DIAU will always adversely impact the phase and amplitude of those increments.

3. Design of idealized two-layer model experiments

a. Two-layer model

The first model used to examine the EnKF with 4DIAU is a dry two-layer primitive equation model (Zou et al. 1993), which was used in Hamill et al. (2001) and Hamill and Whitaker (2005) for ensemble data assimilation experiments. The model is spectral, and the model state vector consists of vorticity and divergence spectral coefficients at two levels and coefficients of layer thickness $\Delta\pi$ for each layer, where π is the Exner function. The sum of the layer thicknesses is the total mass. The temporal evolution of the total mass tendency averaged over the domain can be used as a measure of external mode gravity wave amplitude. We will use this diagnostic to measure the amplitude of imbalances introduced in the data assimilation.

The model parameters are briefly described here. There is a zonal wavenumber-2 terrain, which has a

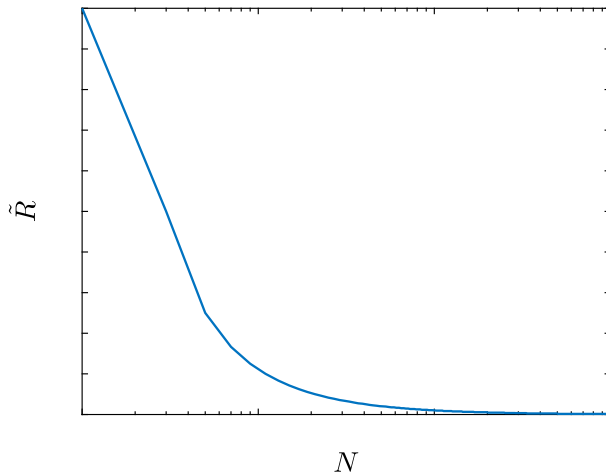


FIG. 2. The ratio \tilde{R} of the integral of IAU forcing for 4DIAU and 3DIAU over the assimilation window and all possible waves as a function of the number of times of the analysis increments N . See (7) in section 2 for more details.

maximum (minimum) amplitude of 2000 (−2000) m at latitudes of 45°N and 45°S and longitudes of 0° and 180° (90° and 270°) and smoothly decreases to 0 m at the poles and equator. The model is forced by Newtonian relaxation to a prescribed interface Exner function with a damping time scale of 20 days. There is ∇^8 hyperdiffusion with a 12-h e -folding time scale used. The other model parameters are the same as in Hamill and Whitaker (2005). The model is run at two triangular truncations: T32 and T42. A fourth-order Runge–Kutta scheme is used for numerical integration, and the steps are 15 min for both resolutions. The error-doubling time of the model at T32 is approximately 4 days.

b. Experimental design

Observing system simulation experiments (OSSEs) are conducted in the two-layer model. Nature runs are created at T32 and T42 resolutions separately. The difference between these two model resolutions will be used to introduce model error due to insufficient model resolution. The ensembles with default size 20 are initialized with random draws from the model climatology. Observations of interface height (unit: m) are generated

by adding errors randomly drawn from $\text{Normal}(0, 1000) \text{ m}^2$ to spatially interpolated values from the nature runs. The observation error variance is about 1% of the globally averaged climatological variance in 12-h forecasts from the natural run at T32. The observations are taken every 12 h at a set of 500 locations that are randomly drawn from 5000 nearly uniformly distributed locations on the sphere. Another set of observations that distribute the 500 observations every 3 h during the 12-h period is also tested, which leads to qualitatively similar results (not shown).

The serial ensemble square root filter (EnSRF; Whitaker and Hamill 2002; Whitaker et al. 2008) is used to assimilate the observations every 12 h. To mitigate spurious correlations due to small ensembles, localization is used to localize the impact of observation on state variables as a function of separation distance. The Gaspari–Cohn (GC; Gaspari and Cohn 1999) localization is adopted here. Covariance inflation is used to maintain appropriate ensemble spread and avoid filter divergence. Multiplicative covariance inflation (Whitaker and Hamill 2012), which inflates the posterior ensemble in proportion to the amount that observations reduce the ensemble spread (relaxation-to-prior spread), is used. Hamill and Whitaker (2005) demonstrated that additive inflation (Mitchell et al. 2002; Houtekamer and Mitchell 2005) was more effective than multiplicative inflation to parameterize the model error resulting from insufficient model resolution. Therefore, additive inflation is applied for the imperfect model experiments (see details below), where perturbations randomly drawn from the climatology of 12-h forecast model error and scaled by the additive inflation value are added to the ensemble prior before the EnSRF update. A database of 12-h forecast model errors is created by computing the difference between 12-h forecasts with the T32 forecast model initialized from the T42 nature run truncated to T32, and the T42 nature run truncated to T32 12 h later.

Three assimilation experiments are conducted: EnKF-RAW, EnKF-3DIAU, and EnKF-4DIAU (details in Table 1). The assimilation experiments are conducted at T32, although the assimilated observations are

TABLE 1. List of experiments.

Expt	Description
EnKF-RAW	Control experiment without any initialization
EnKF-3DIAU	3DIAU is applied, which incorporates the analysis increment at the middle of the assimilation window that is assumed constant over the whole assimilation window
EnKF-4DIAU	4DIAU is applied, which incorporates 3-hourly analysis increments over the whole assimilation window
EnKF-4DIAU _{xH}	Same as EnKF-4DIAU, but using x -hourly ($x = 1$ or 6) analysis increments during an assimilation window
EnKF-DFI	A digital filter with a span of 6 h centered on the 3-hourly forecast is applied

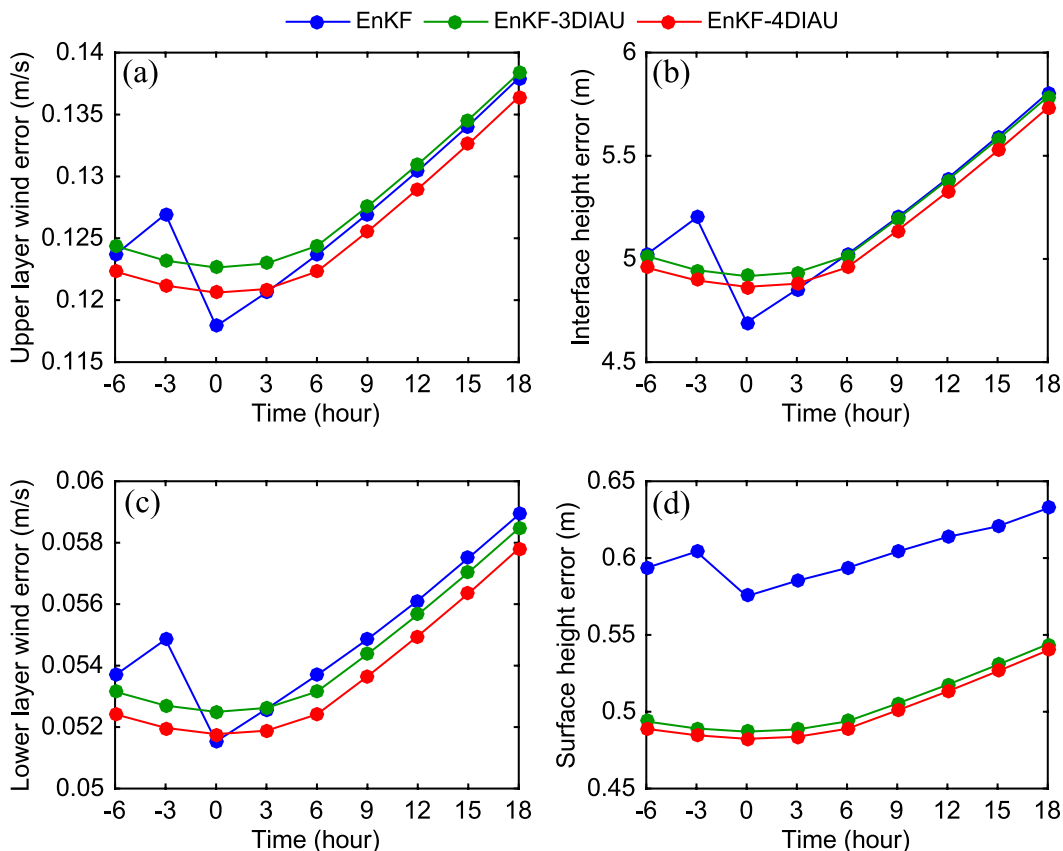


FIG. 3. Mean RMSE in the current (-6 to $+6$ h) and next (6 to 18 h) assimilation windows for (a) upper-level wind, (b) interface height, (c) lower-level wind, and (d) surface height. The forecast model is perfect in these experiments.

generated from the T32 (T42) nature runs for the perfect (imperfect) model experiments. The assimilation parameters (localization, multiplicative inflation, and additive inflation for imperfect model) are tuned to be optimal for each assimilation experiment separately. Each assimilation experiment runs for 3475 update cycles, and the last 2000 cycles are used for verification.

4. Two-layer model results

a. Perfect model experiments

To evaluate the results, the spectral coefficients of vorticity and divergence at two levels and layer thickness for each layer are transformed to u and v winds at two levels and surface and interface pseudoheight. The time-mean value of the root-mean-square error (RMSE) relative to the nature run is computed for ensemble mean winds at each level, surface, and interface pseudoheight separately. Pseudoheight (which is equal to geometric height in an isentropic atmosphere) is related to Exner function π by $z = \theta_1(C_p - \pi)/g$, where θ_1 is the potential temperature of the lower layer, g is

gravity, and C_p is the specific heat of air at constant pressure.

The 3-hourly mean RMSE in the current and next assimilation windows are shown in Fig. 3. During current assimilation window ($-6 \leq t < 6$), EnKF-RAW has an instantaneous error reduction at $t = 0$ h due to the insertion of analysis increments. The RMSE for EnKF with IAU evolves during the assimilation window as the IAU procedure gradually introduces the analysis increments. During the assimilation window, the error with IAU first decreases and then increases, reaching a minimum close to the middle of the assimilation window. One might expect the error to be minimized at the end of the assimilation window, after the application of the IAU forcing is complete. The fact that the error has started to increase before the full IAU forcing has been applied indicates that there is a trade-off between forecast error growth and the inclusion of observation information via the IAU forcing. EnKF-4DIAU has smaller errors than EnKF-3DIAU throughout, demonstrating the advantage of considering the propagation of analysis increments in the assimilation window. EnKF-4DIAU also has smaller errors than EnKF-RAW during

TABLE 2. Mean noise parameters ($\times 10^{-4} \text{ m s}^{-1}$) in the middle of the next assimilation window from different assimilation experiments for perfect and imperfect model assumptions. The first two rows are for the default 20-member ensemble, and the last row is for the 80-member ensemble.

Model error	EnKF-RAW	EnKF-3DIAU	EnKF-4DIAU
No	6.61	6.41	6.41
Yes	99.03	9.00	9.29
No (80 members)	6.04	6.01	6.01

the free forecast over the next assimilation window ($6 \leq t < 18$), indicating that reduction of imbalance through the smooth application of time-varying analysis increments results in more effective assimilation of observations. Errors in the surface height field, which carries the signal of the external gravity mode, are particularly sensitive to imbalance introduced by the assimilation. Both EnKF-3DIAU and EnKF-4DIAU lead to forecast error reductions of nearly 15% for this variable.

Fujita et al. (2007), Jukes and Lawrence (2009), and Lei et al. (2012c) have all shown that imbalances introduced by the intermittent insertion of analysis increments by the EnKF can result in spurious, transient

oscillations such as gravity waves. To measure the imbalance in the model states, a noise parameter that is the time mean domain-averaged absolute value of the total mass tendency is computed. As shown in the first row of Table 2, the noise parameter is smaller for EnKF-3DIAU and EnKF-4DIAU than EnKF-RAW at 12h, reflecting the reduction of imbalances when the IAU is used.

b. Imperfect model experiments

Figure 4 shows 3-hourly mean RMSE in the current and next assimilation windows when model error is present. EnKF-3DIAU and EnKF-4DIAU produce smaller errors than EnKF-RAW for all state variables. The error reduction of EnKF with IAU compared to EnKF-RAW is larger when model error is present (Figs. 3 and 4). Consistent with these results, the noise parameter of EnKF-RAW is an order of magnitude larger than that from the EnKF with IAU (the second row of Table 2), presumably because the observations created from the natural run at T42 resolution are inconsistent with the “slow manifold” of the T32 forecast model attractor.

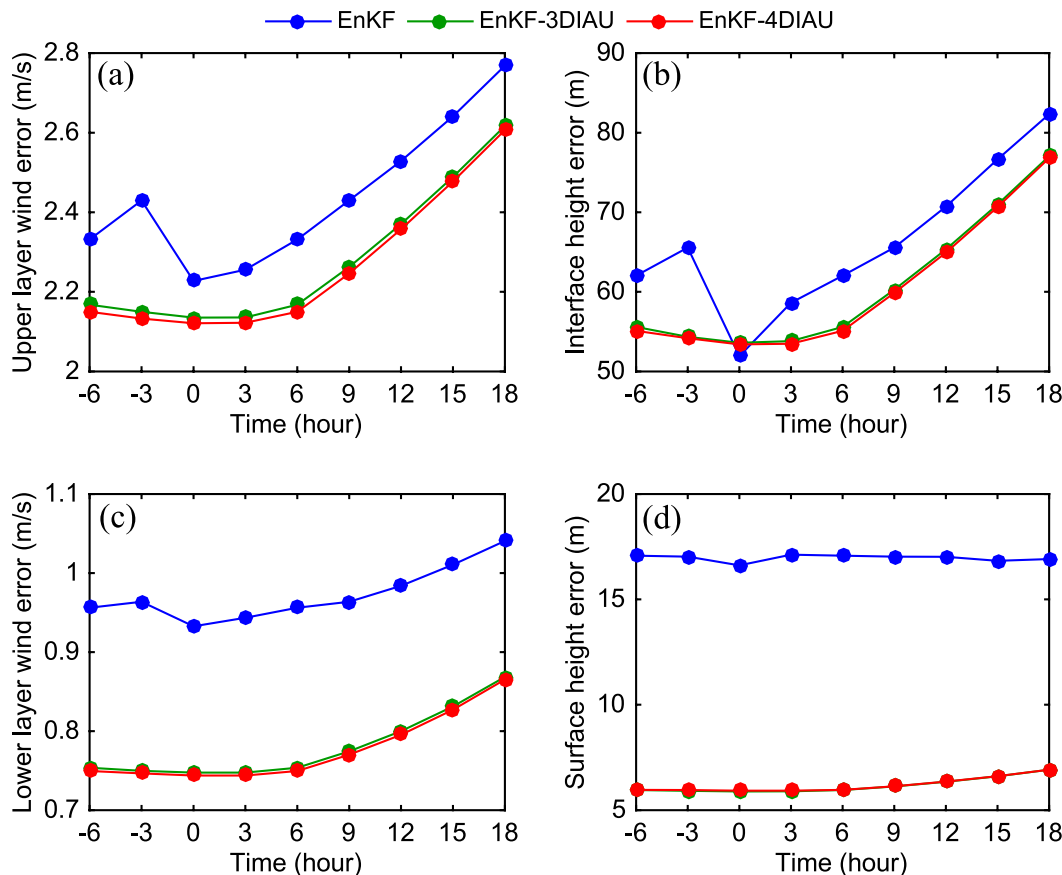


FIG. 4. As in Fig. 3, but using an imperfect forecast model.

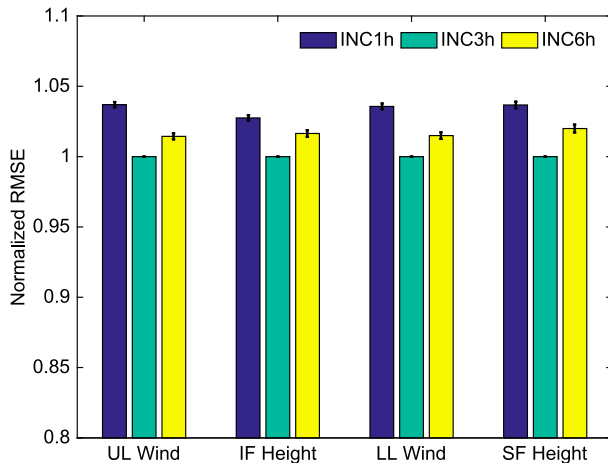


FIG. 5. Mean RMS forecast error in the middle of the next assimilation window (hour 12) for EnKF-4DIAU with different analysis increment frequencies for upper-level wind (UL wind), interface height (IF height), lower-level wind (LL wind), and surface height (SF height). Results are normalized by the mean RMS forecast error for EnKF-4DIAU with 3-hourly analysis increment (INC3h), so that the value plotted for INC3h is always 1. The short black lines at the top of each bar denote the standard deviation of the forecast error.

EnKF-4DIAU has slightly smaller errors for upper- and lower-level winds and interface height than EnKF-3DIAU, while they have nearly the same error of surface height (Fig. 4). These results indicate that the imbalances in the EnKF analyses can be exacerbated by the presence of model error, leading to a larger positive impact of both the 3D and 4D IAU algorithms. However, model error also appears to lessen the impact of using time-varying analysis increments in the IAU, leading to a smaller benefit to 4DIAU relative to 3DIAU.

c. Sensitivity to frequency of analysis increments

The schematic of 4DIAU (Fig. 1) shows that the frequency of analysis increments can vary. The sensitivity of EnKF-4DIAU to the frequency of analysis increment is examined with additional experiments EnKF-4DIAU1H and EnKF-4DIAU6H that utilize hourly and 6-hourly analysis increments, respectively (Table 1). The model is assumed perfect, but similar results are obtained with model error, although the overall sensitivity to the frequency of the analysis increments is smaller.

The mean RMS forecast errors in the middle of the next assimilation window for EnKF-4DIAU with different analysis increment frequencies normalized by the mean RMS forecast error of EnKF-4DIAU are shown in Fig. 5. The experiment with 6-hourly analysis increments (EnKF-4DIAU6H) has slightly larger errors than the experiment with 3-hourly analysis increments

(EnKF-4DIAU), indicating that 3-hourly analysis increments better capture the propagation of analysis increments through the assimilation window. However, hourly analysis increments (EnKF-4DIAU1H) do not improve upon 3-hourly analysis increments. One way to explain this result is that there is a trade-off between sampling error and analysis increment frequency. Higher-frequency analysis increments in 4DIAU better resolve the propagation of analysis increments, but result in less time filtering. If the ensemble size is large enough to accurately estimate the higher-frequency time variations in the analysis increments, this should be beneficial. However, if sampling error dominates those higher frequencies, then the reduced time filtering will result in increased imbalance and gravity wave noise. This explanation is confirmed by experiments with a large ensemble size (80 as in section 4d), where hourly analysis increments slightly improve upon 3-hourly analysis increments for upper- and lower-level winds and interface height. However, even with 80 members, hourly analysis increments slightly degrade the surface height field compared to 3-hourly analysis increments. Since the surface height field is quite sensitive to the amplitude of external gravity wave noise, this is consistent with the fact that hourly analysis increments are less effective at filtering high-frequency gravity waves.

d. Large ensemble size

Keperth (2009) and Greybush et al. (2011) showed that covariance localization could degrade dynamical balances between variables in EnKF analyses. The performance of EnKF-4DIAU is examined here in the absence of model error with a large ensemble size (80 members), which can be run without covariance localization in this idealized system. A relaxation to prior spread inflation coefficient of 0.3 is used to keep the ensemble spread consistent with the analysis error.

Figure 6 shows the evolution of 3-hourly errors over the current and next assimilation windows. EnKF-4DIAU has smaller errors than EnKF-RAW for all variables and forecast lead times. EnKF-3DIAU yields smaller errors than EnKF-RAW for the surface height variable, which is very sensitive to the presence of external gravity wave noise. For all other variables, EnKF-3DIAU has larger errors than EnKF-RAW once the IAU forcing turns off at forecast hour 6. Table 2 (third row) shows that EnKF-4DIAU and EnKF-3DIAU have similar levels of gravity wave noise, and both have slightly less noise than EnKF-RAW, which indicates that imbalances can be excited by sampling errors in the EnKF even in the absence of covariance localization.

The analysis increments of surface height at the beginning, middle, and end of the last assimilation cycle

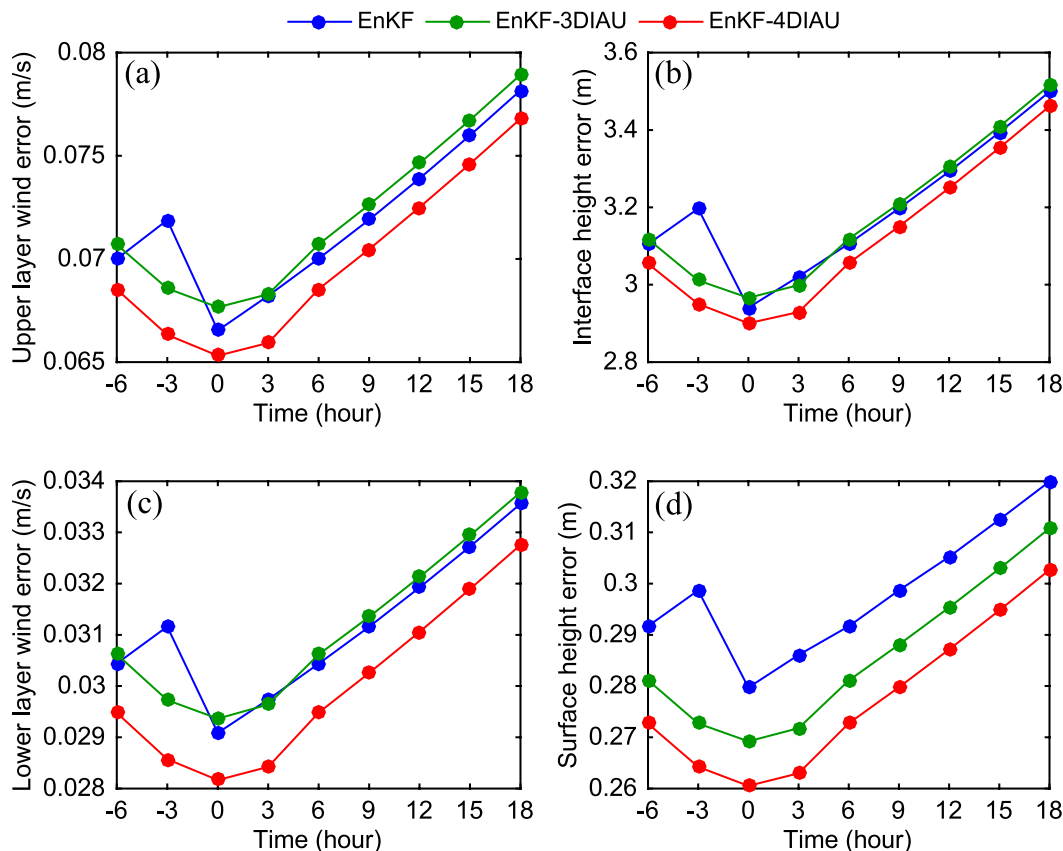


FIG. 6. As in Fig. 3, but for an 80-member ensemble.

from the EnKF-4DIAU experiment are shown in Fig. 7. Only part of the computational domain is shown to clearly show the propagation of analysis increment. As an example, the positive increment with maxima located around (50°N, 75°E) propagates eastward during the 12-h assimilation window, and the positive increment expands with increasing forecast lead times. Similar patterns are obtained for interface height except the sign of increments reverses (not shown).

Although EnKF-3DIAU preserves balance better than EnKF-RAW (Table 2), this can be outweighed by the negative impact of neglecting the time variation of the analysis increment. The relative impact of these effects will depend on the degree of imbalance introduced by the EnKF analysis step, the amplitude of the time-varying component of the analysis increment, and how well the covariances needed to estimate those time variations that can be estimated. In this case, for variables that are less affected by imbalances (such as the upper-layer wind field), the neglect of time variations in the analysis increment in EnKF-3DIAU leads to degraded performance relative to EnKF-RAW. EnKF-4DIAU produces the smallest RMSE for all state variables, indicating that the time-varying component of

the analysis increment can be well estimated in this system with 80 ensemble members (in the absence of model error) and imbalances generated in EnKF-RAW analyses are significantly degrading its performance even in the absence of covariance localization.

5. Design of experiments for the NCEP GFS

The EnKF with 4DIAU is further investigated in the NCEP GFS with real observations. The forecast model is a T574 resolution, 64-level version of the current operational GFS model.

All of the observations used in the NCEP GDAS during 0000 UTC 1 April 2014 and 0000 UTC 8 May 2014 are assimilated every 6 h. A detailed description of these observations that include both conventional and satellite data is available online.¹ The bias correction of satellite radiances is calculated from an experiment that assimilates the same observations using 4DEnVar (Kleist and Ide 2015) with an 80-member ensemble and

¹ See online at http://www.emc.ncep.noaa.gov/mmb/data_processing/prepbufr.doc/table_2.htm and table_18.htm.

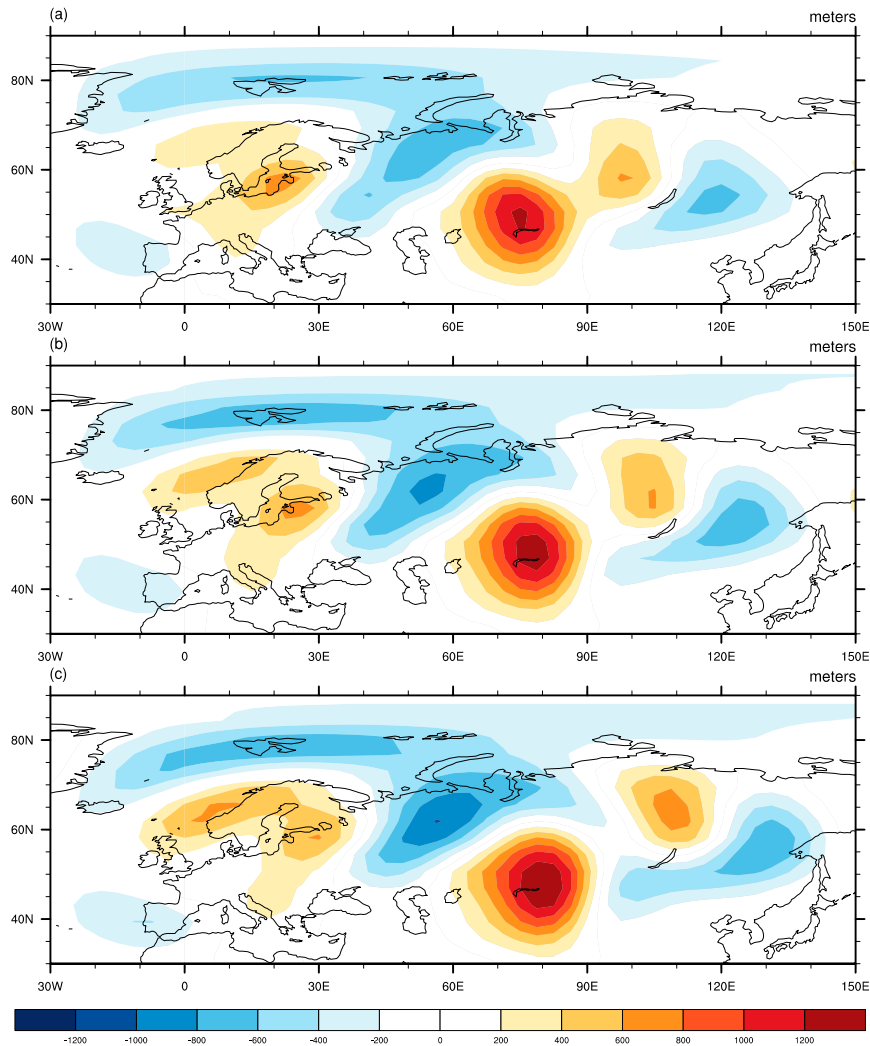


FIG. 7. Snapshots of analysis increment for surface height at (a) -6 , (b) 0 , and (c) 6 h from the last assimilation cycle of the EnKF-4DIAU 80-member ensemble.

no static background error covariance component. The observation forward operator \mathbf{H} is performed by running the Gridpoint Statistical Interpolation analysis system (GSI; Wu et al. 2002; Kleist et al. 2009), saving the values of $\mathbf{H}\mathbf{x}^b$ (where \mathbf{x}^b is the background or prior) without computing the analysis increment. This step is done for the ensemble mean and each ensemble member separately. The observation error covariance \mathbf{R} used is the same as in the NCEP GDAS.

The NOAA operational EnKF (an EnSRF) for the NCEP GFS (NCAR Developmental Testbed Center 2015) is used to assimilate the observations. All assimilation experiments use an 80-member ensemble. The GC localization function is used to mitigate spurious correlations due to limited ensemble size. The observations have no impact on the state variables when the

horizontal (vertical) separation between an observation and a state variable is larger than 1250 km (1.0 scale heights). To maintain appropriate ensemble spread and avoid filter divergence, multiplicative covariance inflation that relaxes posterior ensemble spread back to prior ensemble spread (relaxation-to-prior spread; Whitaker and Hamill 2012) is used, with the relaxation coefficient set to 0.85. Stochastic parameterizations (Palmer et al. 2009) are used to represent model uncertainty within the ensemble forecast step, and no additive inflation is applied.

The assimilation experiments are summarized in Table 1. An additional experiment, not conducted with the two-layer model, is conducted here (EnKF-DFI). It uses a digital filter finalization (DFI) step applied during the first-guess forecasts that filters the total fields over an

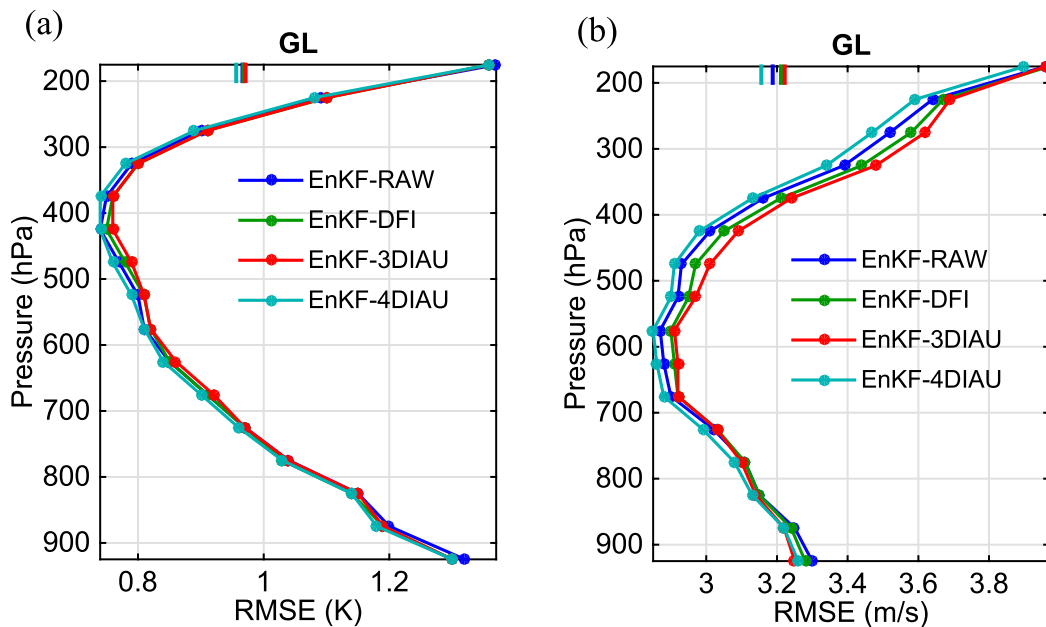


FIG. 8. Time-averaged RMS background forecast observation increment profiles for (a) temperature and (b) wind speed, computed using all in situ observations. The bars on top denote the vertically averaged values.

interval of 6 h, and reinitializes the model at hour 3 using the filtered fields. The same DFI configuration is used in the current operational NCEP GDAS in order to diminish gravity wave oscillations excited by the analysis step. All experiments are run from 0000 UTC 1 April to 0000 UTC 8 May 2014. The first week of assimilation is discarded to avoid transient effects, and the remaining data are used for verification.

6. GFS results

a. Verification against conventional observations

The performance of the assimilation experiments is first evaluated in the observation space. The observation priors from experiments EnKF-RAW, EnKF-DFI, EnKF-3DIAU, and EnKF-4DIAU are subtracted from the in situ conventional observations that include marine and land surface stations, rawinsonde, and aircraft. Figure 8 shows the globally and temporally averaged RMS observation increment profiles for temperature and wind. The bars on top of each panel denote the mean values.

EnKF-4DIAU (EnKF-3DIAU) has the smallest (largest) observation increments, particularly for wind. EnKF-DFI has slightly larger observation increments than EnKF-RAW, and both of them have larger (smaller) observation increments than EnKF-4DIAU (EnKF-3DIAU). In general, the comparisons among

the assimilation experiments are consistent for temperature and wind: EnKF-4DIAU forecasts are the closest to observations, followed by EnKF-RAW, EnKF-DFI, and EnKF-3DIAU.

b. Verification against the ECMWF analyses

Assimilation experiments are verified in model space by evaluating them relative to the ECMWF analyses. The 6-h forecasts are postprocessed to 37 pressure levels between 1000 and 100 hPa on a 1° grid. The 1° gridded forecasts are then evaluated relative to ECMWF 1° gridded analyses. The RMS errors of each experiment relative to the ECMWF analyses are averaged over longitude and the verification period. Considering EnKF-RAW as the control experiment, the differences of the RMS errors between the other experiments and EnKF-RAW are displayed in Fig. 9 for wind speed (qualitatively similar results are obtained for temperature but are not shown). Warm (cold) colors denote EnKF-RAW forecasts that have smaller (larger) RMS errors than the compared experiment.

EnKF-DFI has larger errors in the midlatitudes than EnKF-RAW, especially in the Southern Hemisphere; these larger errors extend from the surface to 200 hPa. The error differences between EnKF-3DIAU and EnKF-RAW are similar to that between EnKF-DFI and EnKF-RAW. EnKF-3DIAU produces larger errors in the southern midlatitudes compared to EnKF-DFI, while it produces smaller errors than EnKF-DFI in the

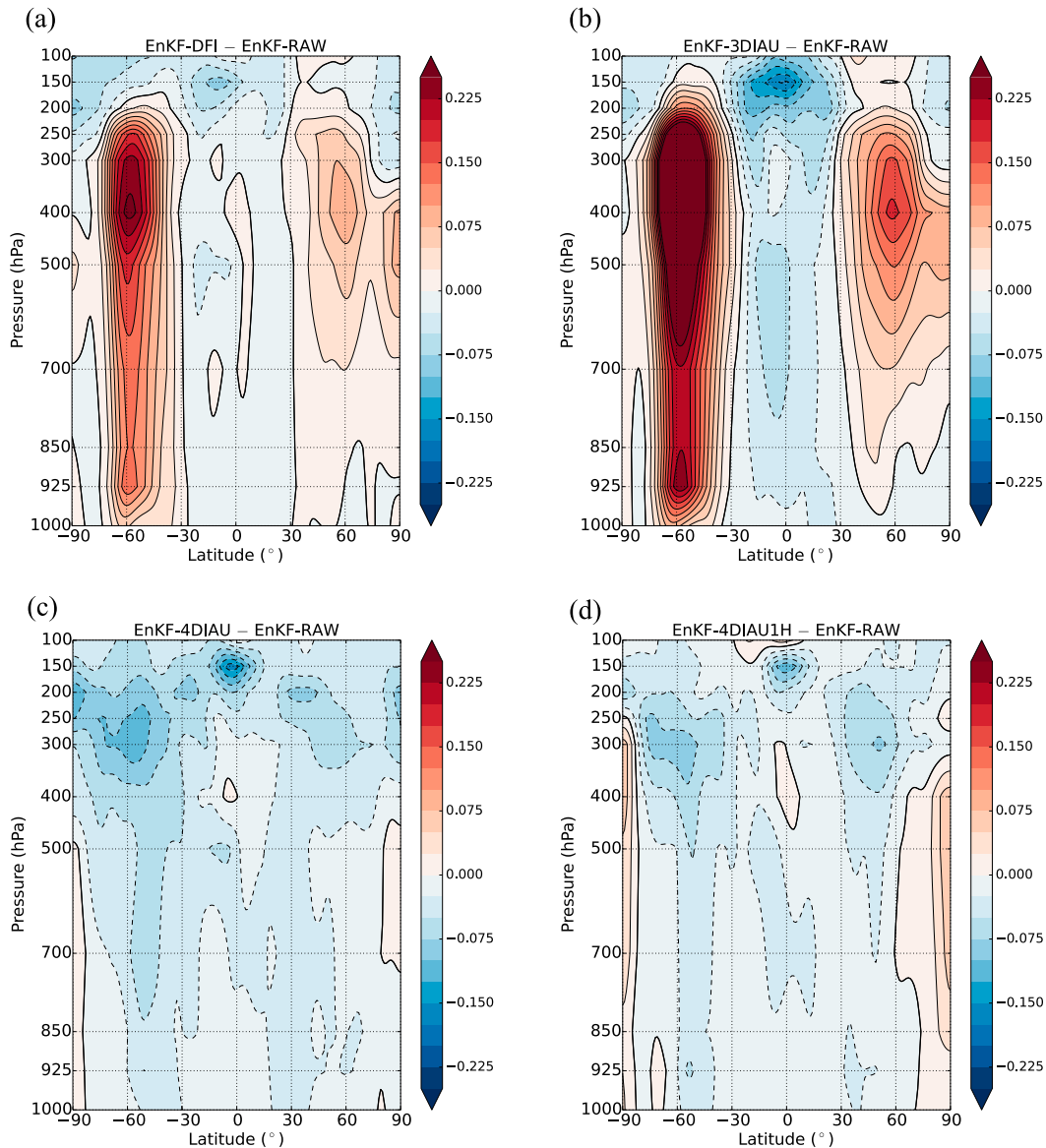


FIG. 9. The RMS error difference of vector wind (unit: m s^{-1}) between experiments (a) EnKF-DFI, (b) EnKF-3DIAU, (c) EnKF-4DIAU, and (d) EnKF-4DIAU1H, and the control experiment EnKF-RAW. The error is computed by verifying the 6-h forecasts from each experiment against the ECMWF analysis. Cold (warm) color means the experiment has smaller (larger) error relative to the ECMWF analysis than the control experiment.

tropics. EnKF-4DIAU produces slightly smaller errors than EnKF-RAW nearly everywhere. Thus, consistent with the observation-based verifications, EnKF-4DIAU forecasts are the closest to ECMWF analyses, followed by EnKF-RAW, EnKF-DFI, and EnKF-3DIAU.

To examine whether the differences of the 6-h forecast errors among the experiments are representative of longer-lead forecasts, a 5-day forecast was launched from each analysis between 0000 UTC 8 April and 0000 UTC 8 May 2014 for each assimilation experiment. The 12-hourly output from the 5-day forecast was verified

against the ECMWF analyses. The cross sections of average RMS error differences for temperature and wind speed at 5-day lead time (not shown) are consistent with those at 6 h (Fig. 9). The temperature error at 500 hPa and wind speed error at 850 hPa at different forecast lead times are shown in Fig. 10. Throughout the 5-day forecast period, EnKF-4DIAU has the smallest forecast error, followed by EnKF-RAW, EnKF-DFI, and EnKF-3DIAU. Similar results are obtained for errors of temperature and wind at the other vertical levels between 1000 and 100 hPa (not shown).

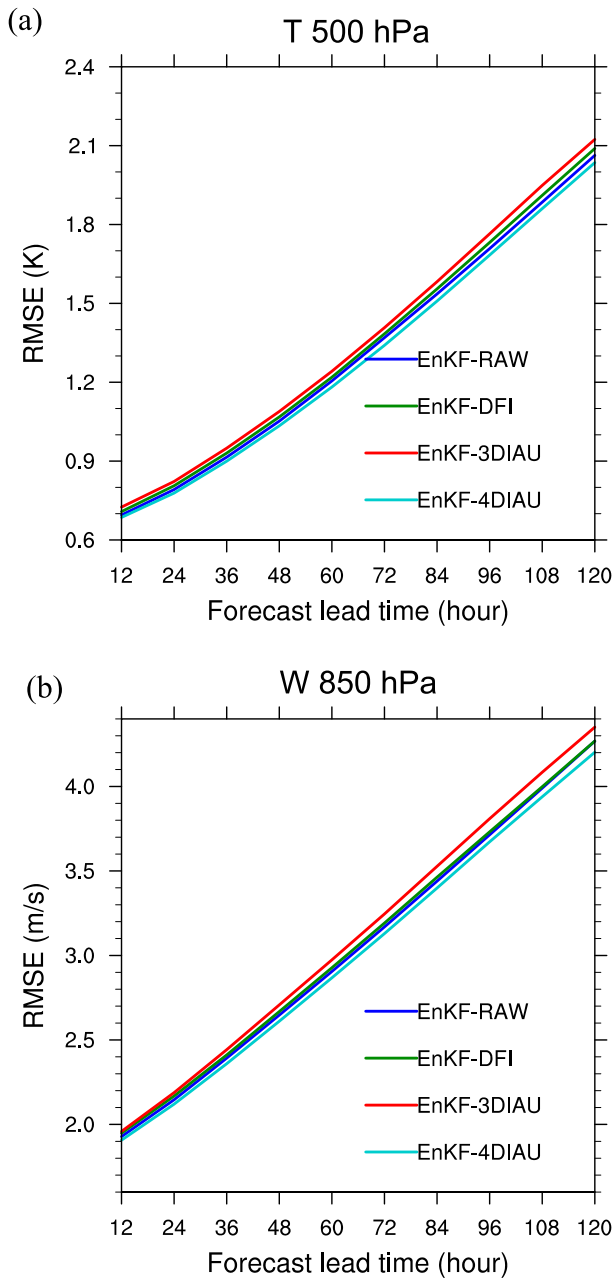


FIG. 10. Temporally and globally averaged forecast errors relative to the ECMWF analyses for (a) temperature at 500 hPa and (b) wind speed at 850 hPa at different lead times.

c. Impact of data assimilation methods on balance

As previously discussed, DFI and IAU are strategies to remedy imbalances introduced by data assimilation. Following Lynch and Huang (1992), the mean absolute tendency of surface pressure is used as the metric to show the amount of imbalance generated by a data assimilation system. The surface pressure tendency between 3- and 0-h forecasts is averaged over the

verification period in the NH, TR, and SH, which is summarized in Table 3.

EnKF-DFI, EnKF-3DIAU, and EnKF-4DIAU have smaller values of surface pressure tendency than EnKF-RAW, indicating that DFI and IAU both help to produce more balanced forecasts. EnKF-3DIAU produces the strongest filtering of high-frequency surface pressure variability, followed by EnKF-DFI and EnKF-4DIAU. As discussed in section 2, 4DIAU acts as a weaker time filter than 3DIAU, because of the time-dependent nature of the 4DIAU forcing (Lorenc et al. 2015; Buehner et al. 2015).

EnKF-DFI and EnKF-3DIAU filter the surface pressure tendencies more in the tropics than in the extratropics (Table 3). This is due to the exaggerated impact of DFI and 3DIAU on atmospheric semidiurnal tidal signals. This is shown in Fig. 11, which presents 3-hourly surface pressure tendencies averaged between 30°S and 30°N and over the verification period for 6-h forecasts initialized at 0000 UTC. The amplitude of the wavenumber-2 semidiurnal tidal signal is reduced significantly in the EnKF-DFI forecast, and even more so in EnKF-3DIAU forecast, as compared to the EnKF-RAW forecast. The tidal signal in EnKF-4DIAU is more similar to EnKF-RAW, consistent with the results of Buehner et al. (2015). Moreover, the tidal signal in the EnKF-3DIAU forecast has slight phase lag compared to the others.

Although EnKF-3DIAU and EnKF-DFI produce more balanced forecasts than EnKF-RAW (Table 3), 3DIAU and DFI can degrade the representation of important phenomena like the semidiurnal tide (Fig. 11). This may be one of the reasons that EnKF-3DIAU and EnKF-DFI have larger errors than EnKF-RAW (sections 6a and 6b).

d. Spinup of total column cloud water

Buehner et al. (2015) suggested that 4DIAU and the recycling of selected physical state variables significantly reduced model spinup in the hydrologic cycle compared to the full-field digital filter. To verify the impact of 4DIAU on the model hydrologic cycle, we have computed the temporally averaged total column cloud condensate for 0-h forecasts (valid at the middle of the IAU window), 3-h forecasts (valid at end of the IAU window), and 6-h forecasts (valid at the middle of the next IAU window). The total column cloud water from EnKF-RAW is 0.14×10^{-3} at lead time 0h, and increases to 0.18×10^{-3} at lead time 3h (~22%) due to model spinup, and increases further between forecast hours 3 and 6 (Fig. 12). EnKF-DFI behaves similarly to EnKF-RAW, while EnKF-3DIAU and EnKF-4DIAU forecasts have larger total column cloud condensate

TABLE 3. Temporally and globally averaged absolute 3-h surface pressure tendency [$\text{hPa} (3\text{ h})^{-1}$] (estimated from the difference between 3- and 0-h forecasts) during the verification period in the Northern Hemisphere (NH), tropics (TP), and Southern Hemisphere (SH) for each assimilation experiment.

	EnKF-RAW	EnKF-DFI	EnKF-3DIAU	EnKF-4DIAU	EnKF-4DIAU1H
NH	1.42	1.15	1.06	1.29	1.28
TR	1.77	1.17	0.91	1.60	1.57
SH	1.78	1.52	1.42	1.68	1.66

throughout the forecast period, particularly at the start of the forecast. This suggests that the IAU does indeed reduce “shock” to the model’s hydrologic cycle introduced by data assimilation. More analysis is needed to determine if the model cloud fields are more realistic in the IAU experiments.

e. Sensitivity to frequency of analysis increments

Results from the two-layer model show that for a 12-h assimilation window, EnKF-4DIAU can be improved with more frequent analysis increments, as long as the temporal covariances can be estimated accurately enough and the imbalance can be effectively constrained. Here the sensitivity of 4DIAU to the frequency of analysis increments is examined by conducting an additional experiment of EnKF-4DIAU with hourly (instead of 3-hourly) analysis increments (EnKF-4DIAU1H), while retaining the 6-h assimilation window. EnKF-4DIAU1H requires the computation of four

more analysis increments than EnKF-4DIAU. However, the extra computational cost can be significantly reduced when the local ensemble transform Kalman filter (LETKF; Hunt et al. 2007) is applied, because the LETKF analysis weights remain constant in an assimilation window and need only be computed once.

Figure 13 shows the globally averaged RMS background forecast observation increments for temperature and wind speed for EnKF-4DIAU and EnKF-4DIAU1H. EnKF-4DIAU1H and EnKF-4DIAU are generally very similar, although the EnKF-4DIAU1H forecasts are slightly closer to wind observations than EnKF-4DIAU above 600 hPa. Figure 9d displays the difference of 6-h forecast vector wind between EnKF-4DIAU1H and EnKF-RAW relative to the ECMWF analyses. Comparing Figs. 9d and 9c, it does not appear that EnKF-4DIAU1H 6-h forecasts are significantly closer to the ECMWF analyses than EnKF-4DIAU. Table 3 and Fig. 11 show that the amplitude of surface pressure tendencies in EnKF-4DIAU1H is similar to EnKF-4DIAU, as is the semidiurnal tidal signal. The

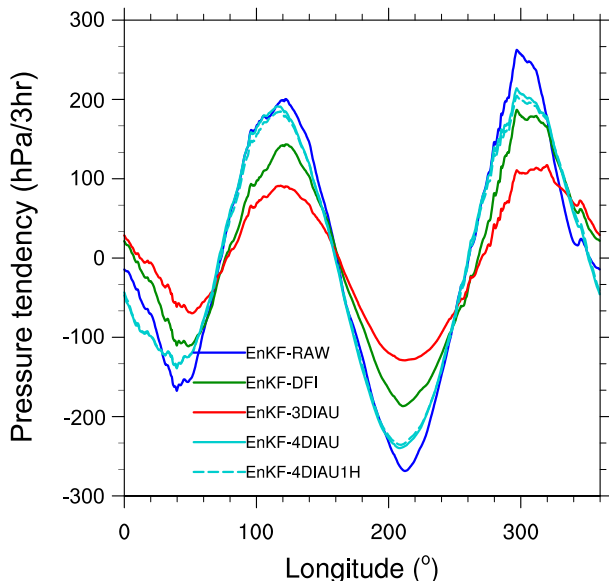


FIG. 11. The semidiurnal tide at 6-h forecast lead time, as measured by 3-hourly surface pressure tendencies averaged between 30°S and 30°N , for forecasts initialized at 0000 UTC and averaged over the verification period for experiments EnKF-RAW, EnKF-DFI, EnKF-3DIAU, EnKF-4DIAU, and EnKF-4DIAU1H.

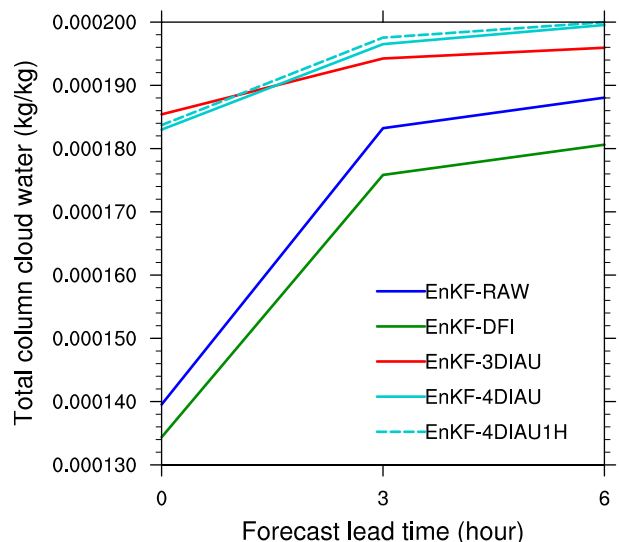


FIG. 12. Total column cloud water averaged over the tropics at forecast lead times 0, 3, and 6 h during the verification period for experiments EnKF-RAW, EnKF-DFI, EnKF-3DIAU, EnKF-4DIAU, and EnKF-4DIAU1H.

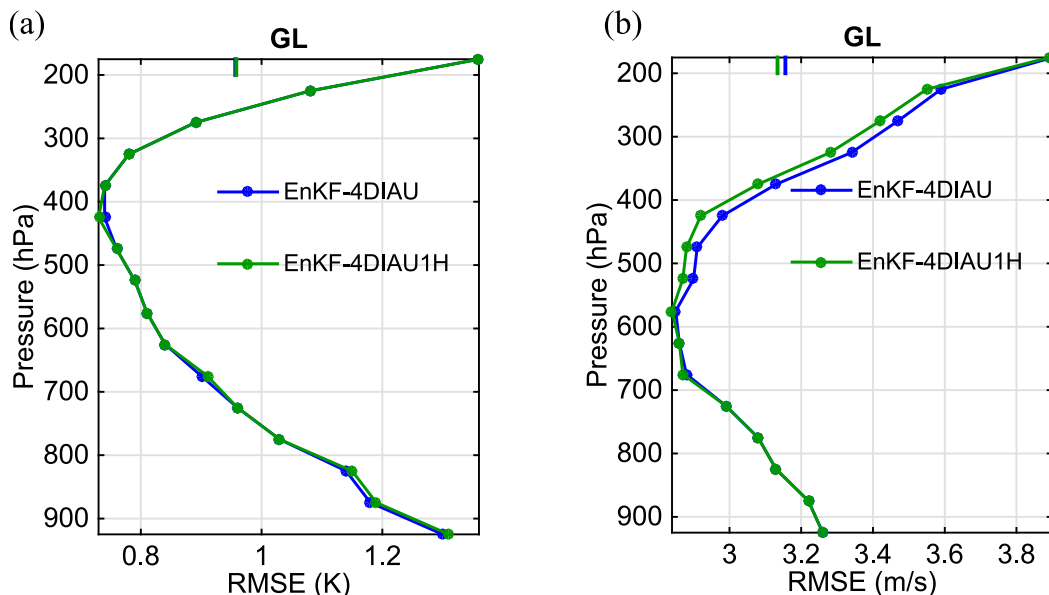


FIG. 13. Vertical profiles of globally averaged RMS background forecast observation increments for all in situ observations of (a) temperature and (b) vector wind for experiments EnKF-4DIAU and EnKF-4DIAU1H. The bars on top denote the vertically averaged values for each experiment.

impact of data assimilation on the spinup of the model total cloud condensate is also similar in EnKF-4DIAU1H and EnKF-4DIAU (Fig. 12). Overall, in the NCEP GFS 80-member EnKF system, there is little difference between using hourly increments and 3-hourly increments in the 4DIAU. Therefore, it appears that the cost of computing the extra increments (and the added IO costs incurrent in the forecast model integration when reading those increments) may not be justified with an 80-member ensemble. However, using hourly increments may still be beneficial when larger ensembles are used in the data assimilation and/or model errors are reduced, since higher-frequency temporal variations in the analysis increments may be more accurately represented.

7. Conclusions

A 4DIAU was recently proposed by Lorenc et al. (2015) to filter out the high-frequency oscillations introduced by poorly balanced four-dimensional ensemble variational (4DEnVar) analyses. Compared to 3DIAU, 4DIAU constructs time-varying analysis increments by applying all observations in an assimilation window. These time-varying analysis increments translate into time-varying forcing terms in the forecast model integration during the application of the IAU. The 4DIAU used with EnKF is discussed in this

paper for an idealized dry two-layer primitive equation model and the NCEP GFS with real observations.

Using the two-layer model, the performance of EnKF with and without IAU is examined with varying frequency of analysis increment, ensemble size, and model error amplitude. Compared to the EnKF-RAW (no IAU), EnKF-4DIAU and EnKF-3DIAU reduce imbalances in the analysis, especially when model error is included. EnKF-4DIAU generally produces smaller errors than either EnKF-RAW or EnKF-3DIAU. Increasing the frequency of the analysis increments used in EnKF-4DIAU generally results in smaller errors, as long as the ensemble size is large enough (and model errors are small enough) so that the temporal covariances needed to estimate the higher-frequency components of the time-varying analysis increments can be estimated accurately and the imbalance can be effectively constrained.

Using the NCEP GFS model with the NOAA operational EnKF, consistent results are obtained when evaluating forecasts relative to observations and ECMWF analyses. EnKF-4DIAU generally produces the more accurate forecasts than EnKF-3DIAU, confirming the benefit of considering the propagation of analysis increments in the assimilation window. Using a full-field digital filter in the EnKF (EnKF-DFI), while effective at suppressing high-frequency oscillations in the forecasts, generally degrades forecasts relative to an EnKF with no IAU and no digital filter (EnKF-RAW).

4DIAU also improves the representation of the semi-diurnal tide, while 3DIAU and 4DIAU both significantly reduce spinup in the forecast model hydrometeor fields.

Results here show that increasing the frequency of analysis increments can improve the performance of the EnKF-4DIAU, as long as sampling error and model error are small enough so the temporal covariances needed to estimate the higher-frequency components of the time-varying analysis increments can be estimated accurately. However, as currently configured (80 ensemble members at T574 resolution) increasing the resolution of the analysis increments from 3 to 1 h appears to only show a benefit in the fit of background forecasts to wind observations above 600 hPa.

Compared to 3DIAU, 4DIAU requires extra computational cost to calculate the additional analyses that are not at the center of an assimilation window. This extra computational cost may be relatively small compared to the model integration, especially when the LETKF algorithm is used.

The IAU window here is set to the same as the length of assimilation window, but there could be sensitivities of the 3DIAU and 4DIAU to the IAU window, which will be explored in future studies. The impacts of assimilation frequency on the performance of 3DIAU and 4DIAU also need further exploration.

Acknowledgments. This work was partially supported by the Disaster Relief Appropriations Act of 2013 (P.L. 113-2), which funded NOAA Research Grant NA14OAR4830123, and by the National Natural Science Foundation of China through Grants 41461164008 and 41130964. Thanks to Chris Snyder and two anonymous reviewers whose valuable comments significantly improved the manuscript.

REFERENCES

- Anderson, J. L., 2001: An ensemble adjustment Kalman filter for data assimilation. *Mon. Wea. Rev.*, **129**, 2884–2903, doi:10.1175/1520-0493(2001)129<2884:AEAKFF>2.0.CO;2.
- , 2009: Spatially and temporally varying adaptive covariance inflation for ensemble filters. *Tellus*, **61A**, 72–83, doi:10.1111/j.1600-0870.2008.00361.x.
- , and S. L. Anderson, 1999: A Monte Carlo implementation of the nonlinear filtering problem to produce ensemble assimilations and forecasts. *Mon. Wea. Rev.*, **127**, 2741–2758, doi:10.1175/1520-0493(1999)127<2741:AMCIOT>2.0.CO;2.
- Baer, F., and J. Tribbia, 1977: On complete filtering of gravity modes through non-linear initialization. *Mon. Wea. Rev.*, **105**, 1536–1539, doi:10.1175/1520-0493(1977)105<1536:OCFOGM>2.0.CO;2.
- Bergemann, K., and S. Reich, 2010: A mollified ensemble Kalman filter. *Quart. J. Roy. Meteor. Soc.*, **136**, 1636–1643, doi:10.1002/qj.672.
- Bloom, S. C., L. L. Takacs, A. M. Da Silva, and D. Ledvina, 1996: Data assimilation using incremental analysis updates. *Mon. Wea. Rev.*, **124**, 1256–1271, doi:10.1175/1520-0493(1996)124<1256:DAUIAU>2.0.CO;2.
- Buehner, M., P. L. Houtekamer, C. Charette, H. L. Mitchell, and B. He, 2010a: Intercomparison of variational data assimilation and the ensemble Kalman filter for global deterministic NWP. Part I: Description and single-observation experiments. *Mon. Wea. Rev.*, **138**, 1550–1566, doi:10.1175/2009MWR3157.1.
- , —, —, —, and —, 2010b: Intercomparison of variational data assimilation and the ensemble Kalman filter for global deterministic NWP. Part II: One-month experiments with real observations. *Mon. Wea. Rev.*, **138**, 1567–1586, doi:10.1175/2009MWR3158.1.
- , and Coauthors, 2015: Implementation of deterministic weather forecasting systems based on ensemble-variational data assimilation at Environment Canada. Part I: The global system. *Mon. Wea. Rev.*, **143**, 2532–2559, doi:10.1175/MWR-D-14-00354.1.
- Burgers, G., P. J. van Leeuwen, and G. Evensen, 1998: Analysis scheme in the ensemble Kalman filter. *Mon. Wea. Rev.*, **126**, 1719–1724, doi:10.1175/1520-0493(1998)126<1719:ASITEK>2.0.CO;2.
- Carton, J. A., G. Chepurin, X. Cao, and B. Giese, 2000: A Simple Ocean Data Assimilation analysis of the global upper ocean 1950–95. Part I: Methodology. *J. Phys. Oceanogr.*, **30**, 294–309, doi:10.1175/1520-0485(2000)030<0294:ASODAA>2.0.CO;2.
- Courtier, P., and Coauthors, 1998: The ECMWF implementation of three-dimensional variational assimilation (3D-Var). I: Formulation. *Quart. J. Roy. Meteor. Soc.*, **124**, 1783–1808, doi:10.1002/qj.49712455002.
- Evensen, G., 1994: Sequential data assimilation with a nonlinear quasi-geostrophic model using Monte Carlo methods to forecast error statistics. *J. Geophys. Res.*, **99**, 10 143–10 162, doi:10.1029/94JC00572.
- Fujita, T., D. J. Stensrud, and D. C. Dowell, 2007: Surface data assimilation using an ensemble Kalman filter approach with initial condition and model physics uncertainties. *Mon. Wea. Rev.*, **135**, 1846–1868, doi:10.1175/MWR3391.1.
- Gaspari, G., and S. E. Cohn, 1999: Construction of correlation functions in two and three dimensions. *Quart. J. Roy. Meteor. Soc.*, **125**, 723–757, doi:10.1002/qj.49712555417.
- Gottwald, G. A., 2014: Controlling balance in an ensemble Kalman filter. *Nonlinear Processes Geophys.*, **21**, 417–426, doi:10.5194/npg-21-417-2014.
- Greybush, S. J., E. Kalnay, T. Miyoshi, K. Ide, and B. R. Hunt, 2011: Balance and ensemble Kalman filter localization techniques. *Mon. Wea. Rev.*, **139**, 511–522, doi:10.1175/2010MWR3328.1.
- Hamill, T. M., and J. S. Whitaker, 2005: Accounting for the error due to unresolved scales in ensemble data assimilation: A comparison of different approaches. *Mon. Wea. Rev.*, **133**, 3132–3147, doi:10.1175/MWR3020.1.
- , —, and C. Snyder, 2001: Distance-dependent filtering of background-error covariance estimates in an ensemble Kalman filter. *Mon. Wea. Rev.*, **129**, 2776–2790, doi:10.1175/1520-0493(2001)129<2776:DDFOBE>2.0.CO;2.
- Houtekamer, P. L., and H. L. Mitchell, 2001: A sequential ensemble Kalman filter for atmospheric data assimilation. *Mon. Wea. Rev.*, **129**, 123–137, doi:10.1175/1520-0493(2001)129<0123:ASEKFF>2.0.CO;2.
- , and —, 2005: Ensemble Kalman filtering. *Quart. J. Roy. Meteor. Soc.*, **131**, 3269–3289, doi:10.1256/qj.05.135.
- Huang, B., J. L. Kinter III, and P. S. Schopf, 2002: Ocean data assimilation using intermittent analyses and continuous model

- error correction. *Adv. Atmos. Sci.*, **19**, 965–993, doi:10.1007/s00376-002-0059-z.
- Huang, X.-Y., and P. Lynch, 1993: Diabatic digital-filtering initialization: Application to the HIRLAM model. *Mon. Wea. Rev.*, **121**, 589–603, doi:10.1175/1520-0493(1993)121<0589:DDFIAT>2.0.CO;2.
- Hunt, B. R., E. J. Kostelich, and I. Szunyogh, 2007: Efficient data assimilation for spatiotemporal chaos: A local ensemble transform Kalman filter. *Physica D*, **230**, 112–126, doi:10.1016/j.physd.2006.11.008.
- Juckes, M., and B. Lawrence, 2009: Inferred variables in data assimilation: Quantifying sensitivity to inaccurate error statistics. *Tellus*, **61A**, 129–143, doi:10.1111/j.1600-0870.2008.00376.x.
- Kalman, R. E., 1960: A new approach to linear filtering and prediction problems. *J. Basic Eng.*, **82**, 35–45, doi:10.1115/1.3662552.
- Kalnay, E., 2002: *Atmospheric Modeling, Data Assimilation and Predictability*. Cambridge University Press, 368 pp.
- Kepernt, J., 2009: Covariance localisation and balance in an ensemble Kalman filter. *Quart. J. Roy. Meteor. Soc.*, **135**, 1157–1176, doi:10.1002/qj.443.
- Kleist, D. T., and K. Ide, 2015: An OSSE-based evaluation of hybrid variational–ensemble data assimilation for the NCEP GFS. Part II: 4DEnVar and hybrid variants. *Mon. Wea. Rev.*, **143**, 452–470, doi:10.1175/MWR-D-13-00350.1.
- , D. F. Parrish, J. C. Derber, R. Treadon, W. Wu, and S. Lord, 2009: Introduction of the GSI into NCEP Global Data Assimilation System. *Wea. Forecasting*, **24**, 1691–1705, doi:10.1175/2009WAF2222201.1.
- Lei, L., D. R. Stauffer, S. E. Haupt, and G. S. Young, 2012a: A hybrid nudging-ensemble Kalman filter approach to data assimilation. Part I: Application in the Lorenz system. *Tellus*, **64A**, 18484, doi:10.3402/tellusa.v64i0.18484.
- , —, and A. Deng, 2012b: A hybrid nudging-ensemble Kalman filter approach to data assimilation. Part II: Application in a shallow-water model. *Tellus*, **64A**, 18485, doi:10.3402/tellusa.v64i0.18485.
- , —, and —, 2012c: A hybrid nudging-ensemble Kalman filter approach to data assimilation in WRF/DART. *Quart. J. Roy. Meteor. Soc.*, **138**, 2066–2078, doi:10.1002/qj.1939.
- Lorenc, A. C., 1986: Analysis methods for numerical weather prediction. *Quart. J. Roy. Meteor. Soc.*, **112**, 1177–1194, doi:10.1002/qj.49711247414.
- , N. Bowler, A. Clayton, S. Pring, and D. Fairbairn, 2015: Comparison of hybrid-4DEnVar and hybrid-4DVar data assimilation methods for global NWP. *Mon. Wea. Rev.*, **143**, 212–229, doi:10.1175/MWR-D-14-00195.1.
- Lynch, P., and X.-Y. Huang, 1992: Initialization of the HIRLAM model using a digital filter. *Mon. Wea. Rev.*, **120**, 1019–1034, doi:10.1175/1520-0493(1992)120<1019:IOTHMU>2.0.CO;2.
- Machenhauer, B., 1977: On the dynamics of gravity oscillations in a shallow water model with applications to normal mode initialization. *Contrib. Atmos. Phys.*, **50**, 253–271.
- Mitchell, H. L., P. L. Houtekamer, and G. Pellerin, 2002: Ensemble size, balance, and model-error representation in an ensemble Kalman filter. *Mon. Wea. Rev.*, **130**, 2791–2808, doi:10.1175/1520-0493(2002)130<2791:ESBAME>2.0.CO;2.
- NCAR Developmental Testbed Center, 2015: NOAA ensemble Kalman filter (beta release v1.0 compatible with GSI community release v3.3) user's guide. NCAR, 55 pp. [Available online at http://www.dtcenter.org/com-GSI/users/docs/enkf_users_guide/EnKF_UserGuide_v1.0Beta.pdf.]
- Ourmières, Y., J.-M. Brankart, L. Berline, P. Brasseur, and J. Verron, 2006: Incremental analysis update implementation into a sequential ocean data assimilation system. *J. Atmos. Oceanic Technol.*, **23**, 1729–1744, doi:10.1175/JTECH1947.1.
- Palmer, T., R. Buizza, F. Doblas-Reyes, T. Jung, M. Leutbecher, G. Shutts, M. Steinheimer, and A. Weisheimer, 2009: Stochastic parameterization and model uncertainty. ECMWF Tech. Memo. 598, 42 pp.
- Polavarapu, S., S. Ren, A. M. Clayton, D. Sankey, and Y. Rochon, 2004: On the relationship between incremental analysis updating and incremental digital filtering. *Mon. Wea. Rev.*, **132**, 2495–2502, doi:10.1175/1520-0493(2004)132<2495:OTRBA>2.0.CO;2.
- Rienecker, M., and Coauthors, 2007: The GEOS-5 data assimilation system—Documentation of versions 5.0.1 and 5.1.0. NASA GSFC Tech. Rep. Series on Global Modeling and Data Assimilation, NASA/TM-2007-104606, Vol. 27, 92 pp.
- Thepaut, J.-N., R. Hoffman, and P. Courtier, 1993: Interactions of dynamics and observations in a four-dimensional variational data assimilation. *Mon. Wea. Rev.*, **121**, 3393–3414, doi:10.1175/1520-0493(1993)121<3393:IODAOI>2.0.CO;2.
- Wang, X., and T. Lei, 2014: GSI-based four-dimensional ensemble-variational (4DEnsVar) data assimilation: Formulation and single-resolution experiments with real data for NCEP Global Forecast System. *Mon. Wea. Rev.*, **142**, 3303–3325, doi:10.1175/MWR-D-13-00303.1.
- , D. Parrish, D. Kleist, and J. S. Whitaker, 2013: GSI 3DVar-based ensemble-variational hybrid data assimilation for NCEP Global Forecast System: Single-resolution experiments. *Mon. Wea. Rev.*, **141**, 4098–4117, doi:10.1175/MWR-D-12-00141.1.
- Whitaker, J. S., and T. M. Hamill, 2002: Ensemble data assimilation without perturbed observations. *Mon. Wea. Rev.*, **130**, 1913–1924, doi:10.1175/1520-0493(2002)130<1913:EDAWPO>2.0.CO;2.
- , and —, 2012: Evaluating methods to account for system errors in ensemble data assimilation. *Mon. Wea. Rev.*, **140**, 3078–3089, doi:10.1175/MWR-D-11-00276.1.
- , —, X. Wei, Y. Song, and Z. Toth, 2008: Ensemble data assimilation with the NCEP Global Forecast System. *Mon. Wea. Rev.*, **136**, 463–482, doi:10.1175/2007MWR2018.1.
- Wu, W. S., R. J. Purser, and D. F. Parrish, 2002: Three-dimensional variational analysis with spatially inhomogeneous covariances. *Mon. Wea. Rev.*, **130**, 2905–2916, doi:10.1175/1520-0493(2002)130<2905:TDVAWS>2.0.CO;2.
- Yan, Y., A. Barth, and J. M. Beckers, 2014: Comparison of different assimilation schemes in a sequential Kalman filter system. *Ocean Modell.*, **73**, 123–137, doi:10.1016/j.ocemod.2013.11.002.
- Zhang, F., C. Snyder, and J. Sun, 2004: Impacts of initial estimate and observation availability on convective-scale data assimilation with ensemble Kalman filter. *Mon. Wea. Rev.*, **132**, 1238–1253, doi:10.1175/1520-0493(2004)132<1238:IOIEAO>2.0.CO;2.
- Zhu, Y., R. Todling, J. Guo, S. E. Cohn, I. M. Navon, and Y. Yang, 2003: The GEOS-3 Retrospective Data Assimilation System: The 6-hour lag case. *Mon. Wea. Rev.*, **131**, 2129–2150, doi:10.1175/1520-0493(2003)131<2129:TGRDAS>2.0.CO;2.
- Zou, X., A. Barcilon, I. M. Navon, J. Whitaker, and D. G. Cacuci, 1993: An adjoint sensitivity study of blocking in a two-layer isentropic model. *Mon. Wea. Rev.*, **121**, 2833–2857, doi:10.1175/1520-0493(1993)121<2833:AASSOB>2.0.CO;2.